applied sciences

MDPI

Article

Impact of Beam Shape and Frequency on Weld Seam Geometry and Penetration Depth Using a Coherent Beam Combining Laser

Karthik Ravi Krishna Murthy *, Reza Sanei, Abhay Sharma, Simon Olschok and Uwe Reisgen

Welding and Joining Institute, RWTH Aachen University, 52062 Aachen, Germany
* Correspondence: karthik.krishnamurthy@isf.rwth-aachen.de

Abstract

The geometry and quality of a weld seam are critical factors in laser beam welding, influencing mechanical performance and structural integrity. Dynamically modulated laser beams provide a precise means of tailoring energy input in high-power laser welding processes. This study investigates the influence of beam shape and modulated frequency on weld seam geometry, penetration depth, and capillary behaviour using a coherent beam combining (CBC) laser system from Civan Lasers. Three beam intensity distributions—single point, line–point–line (LPL), and boomerang—were applied across a modulation frequency range of 1, 10, and 100 kHz during the welding of duplex and austenitic stainless steels. High-speed imaging captured real-time capillary dynamics, and the data were analysed to assess capillary stability, measure capillary diameter, and determine the capillary front angle as a function of frequency and beam shape. Transverse cross-sections of the welds were prepared to evaluate seam geometry and microstructure. The results show that beam shape significantly affects energy distribution and weld profile, while modulation frequency critically influences capillary behaviour and penetration characteristics. These findings highlight the critical role of dynamic beam shaping and frequency modulation in optimizing laser welding processes for material-specific performance, offering a versatile platform for advancing precision manufacturing using CBC technology.

Keywords: coherent beam combining; beam shape; beam frequency; capillary behaviour; penetration characteristics; microstructure

check for updates

Academic Editor: Wilma Polini

Received: 21 June 2025
Revised: 24 July 2025
Accepted: 29 July 2025
Published: 28 August 2025

Citation: Krishna Murthy, K.R.; Sanei, R.; Sharma, A.; Olschok, S.; Reisgen, U. Impact of Beam Shape and Frequency on Weld Seam Geometry and Penetration Depth Using a Coherent Beam Combining Laser. *Appl. Sci.* **2025**, *15*, 9432. https://doi.org/10.3390/app15179432

Copyright: © 2025 by the authors. Licensee MDPI, Basel, Switzerland. This article is an open access article distributed under the terms and conditions of the Creative Commons Attribution (CC BY) license (https://creativecommons.org/licenses/by/4.0/).

1. Introduction

Laser beam welding is widely recognised as a high-precision joining technique that is particularly suited for applications demanding high mechanical strength and structural reliability. Its key advantages include confined fusion and heat-affected zones and minimal thermal distortion, which make it an ideal process for welding advanced and high-performance alloys [1,2]. Weld seam geometry and quality play a vital role in ensuring both the functionality and durability of safety-relevant components. Achieving consistent seam formation requires precise control of energy input, which depends on multiple factors including welding speed, laser wavelength, shielding conditions, and, most critically, the spatial intensity distribution of the laser beam on the workpiece. This intensity profile governs the local heat distribution, which significantly influences capillary formation and stability, and thus directly affects the weld quality [3,4]. While Marangoni convection is the dominant mechanism driving melt pool flow in conduction mode laser welding, the transition to the keyhole regime introduces additional influencing forces, including recoil pressure, vapour-induced shear stress, and capillary effects, resulting in significantly more

complex melt flow behaviour [5]. However, keyhole stability in the melt pool is widely recognised as a primary determinant of weld quality in deep penetration laser welding processes [6].

1.1. Research Background

High-energy welding processes benefit significantly from the ability to dynamically modulate the laser beam, which enables spatially and temporally resolved control of heat distribution in the workpiece. Dynamic beam shaping (DBS) has emerged as a promising technique in this context, offering innovative approaches to process control, particularly by modifying temperature gradients during the cooling phase, which, for example, can help in reducing hot-cracking in Al-alloys via beam shapes generated by laser beam oscillation [7]. Coherent beam combining (CBC) represents a more complex strategy in this category, enabling the customization of beam intensity profiles to achieve targeted melt pool dynamics and enhance overall welding quality. In order to form a CBC laser, the outputs of several single-mode fibre lasers (array) are combined while their light waves remain in phase. Using optical phase modulators, the electromagnetic waves reinforce each other constructively upon the target. The outputs are sorted in a two-dimensional array (optical phased array—OPA), and their beams are optically overlapped into one strong laser beam at a desirable focus point. This enables higher power, high beam quality, and—most importantly—dynamic control over the beam's phase, shape, and direction. What makes these types of lasers unique is their ability to create different types of intensity distributions (beam shapes), from classic spots, rings, and multiple spots to whole lines and complex shapes, and to change them practically in real time without relying on expensive and maintenance-intensive optics to generate mostly static, non-complex beam shapes, as is the case with conventional lasers. For instance, the maximum modulation frequency of OPA CBC lasers is 80 MHz, while the shortest possible lifetime of a single point is only 12.5 ns. For Civan CBC lasers in particular, a shape can consist of a maximum number of 1024 single points, while it is also possible to generate a sequence of up to 14 different shapes. For example, these shapes can be used for controlling the melt pool in the laser welding of copper, a material known for high thermal conductivity and difficult-to-weld melt pool viscosity [8,9]. It is also notable that this type of laser system does not need any mechanical mirrors or galvos to focus steering (unlike conventional lasers), since its phase control is electronic. This enables it to compete with welding strategies that were previously used mainly in electron beam welding (e.g., stirring the heat distribution in a weld pool in real time). Additionally, the used Civan laser system is capable of dynamically switching between beam patterns in real time, ranging from microseconds to several MHz. This gives the user an additional level of control over the laser welding process that goes beyond the capabilities of conventional lasers and other CBC systems, opening up a major research gap in the field of capillary, material, and weld seam geometry control. CBC lasers are capable of generating variable intensity distributions at high power levels. By combining tailored beam shapes with defined modulation frequencies, the beam–material interaction can be selectively adjusted to control melt pool dynamics and capillary behaviour [9–12]. This, in turn, has a direct impact on the resulting weld seam geometry. Troise et al. state that beam shapes such as the "boomerang" widen the weld seam and reduce the size of the upper bead, while there are significant differences when changing the frequency at which the shape is generated between 0.1 and 100 kHz. The higher frequency does lead to a coarser grain and a very wide heat-affected zone (HEZ) [13]. Active control of capillary behaviour is crucial, since the collapse of the keyhole may result in defects such as porosity and spatter-induced blow-outs [14]. Another capillary-related issue—although already problematic for conventional lasers— that can negatively influence welding results

with CBC lasers is the sensitivity of the projected beam shape to process plume during deep penetration welding. It can be controlled using a cross-jet placed directly above the workpiece, so that no welding fumes cross the beam path [15,16]. Table 1 summarizes a short selection of works relevant to this field.

Table 1. A selection of previous work in this field.

Reference	Beam Shaping Technology	Power [kW]	Material	Scope of Work/Influence on
[3]	FRM	4	Pure Nickel	Process dynamics
[7]	DBS Oscillated	5	Al-alloys	Hot crack sensitivity
[9]	DPS OPA	14	Stainless	Technology Benchmark
[8]	DBS OPA	14	Copper	Melt pool control
[13]	DBS OPA	14	Steel	Seam & melt pool geometry
[17]	FRM	2.4	Stainless	Capillary depth fluctuation
[18]	FRM	4	Stainless	Microstructure & mechanical prop.

1.2. Related Research

To date, efforts to specifically manipulate capillary behaviour by modulating intensity distributions have predominantly employed combinations of ring and core lasers as well as flexible ring mode lasers (FRMs) or classic oscillation [3,7]. For example, Xie et al. stated that for stainless steel, the ring part of an FRM laser is not only capable of reducing welding spatter but also has a notable impact on columnar grain size and ferrite density. This is explained by the lower temperature gradient in the melt pool, which is due to a diluted heat source that is achievable with an FRM laser [18]. An even simpler approach to adding a ring laser source to a central core laser can benefit the welding process, as shown by Zaiß et al., and therefore improve the welding results. This welding strategy can reduce capillary fluctuation through the production of a wider melt pool and a deceleration of melt velocities, which is beneficial for high–speed laser welding of stainless steel [17]. As previously mentioned, these strategies primarily aim to stabilize the capillary and prevent its collapse—a key mechanism underlying welding defects such as porosity and spatter in deep penetration laser welding [19]. It is worth noting that beam shaping influences not only capillary stability but also the spatial characteristics of the melt pool [20–22]. The complex process of scanning a dynamic beam shape can be compared to the simpler circular oscillation employed in conventional laser scanners. While the latter is generally considered a less sophisticated approach, it still enables effective control of capillary and melt pool behaviour, contributing to pore reduction and enhanced degassing [23]. Oscillating and stirring of the laser beam further contribute to a reduction in temperature gradients and melt pool flow velocities, which can in turn lead to improved weld quality [24]. As shown in many research articles—both experimental and simulated—a direct correlation between capillary and seam geometry can easily be drawn. The shape and depth of the capillary changes with the welding speed, which in turn affects the resulting weld penetration depth and seam shape, as well as the frequency of welding defects such as porosity [9,11,25,26]. This can also be influenced by the intensity distribution. Among other things, ray tracing of the laser radiation arriving on the surface also plays a role here, as it is absorbed and reflected back to varying degrees depending on the actual condition of the capillary. The influence of the metal vapour plume on the beam reflection in the keyhole should also not be neglected. Furthermore, different intensity distributions not only affect the weld seam

geometry but also lead to the development of distinct grain structures. This is attributed to variations in melt pool morphology and thermal gradients, which govern the direction and mode of grain growth during solidification [27–29]. The heat input—adjustable via laser intensity distribution in conjunction with power and travel speed or with varying oscillation diameters—plays a key role in determining the microstructure of stainless steels. In duplex stainless steels, the resulting phase balance is influenced not only by alloy composition but also by cooling conditions; elevated heat input promotes austenite formation by lowering the ferrite fraction through reduced cooling rates [30,31]. Ferrite in austenitic stainless steels exhibits a higher solubility for impurities such as sulfur and phosphorus. This helps to reduce their segregation into interdendritic regions, where the formation of low-melting-point phases can promote hot cracking and degrade mechanical properties. In duplex stainless steels, however, an excessive ferrite content can impair both corrosion resistance and toughness. Therefore, precise control of the ferrite fraction is essential. While the ferrite–austenite balance is primarily determined by the steel's chemical composition, in duplex steels it can also be influenced by cooling rates, particularly when the preceding heat input is relatively high [32].

1.3. Significance of the Work

Considering the state of the art regarding investigations of the impact of beam shape and frequency on weld seam geometry and penetration depth, to date, studies have mostly focused on simple beam shapes and slower oscillation frequencies or materials other than stainless steel (primarily copper and aluminium), which (by design) do not take into account the simultaneous influence of complex CBC-generated beam shapes and their high frequency oscillation on the steel's austenite–ferrite ratios. While the influence of conventional oscillation and non-CBC beam shaping strategies on cooling rates and the microstructure of stainless steels is fairly well investigated, there is an inescapable research gap regarding investigations of the behaviour of stainless steels in response to complex shape–sequence–frequency combinations that are only achievable with specialized CBC systems such as the Civan Laser System. Therefore, there is a clear need for more in-depth research regarding the contributions that Civan's significantly more complex CBC lasers can make to topics such as capillary control and dimensions, weld seam geometry, the resulting microstructure. Moreover, it is essential to identify and understand the novel challenges introduced by the increased number of adjustable parameters and the high dynamic behaviour inherent to the Civan CBC process, both from a research and application standpoint. Additionally, investigations are required to determine which specific combinations of beam shape, sequence, and oscillation—particularly those not applicable to conventional systems—can provide the greatest possible control of the most important weld pool properties, and which are fundamental for the subsequent welding result. In this context, the simultaneity of the available combinations and the ability to switch between them in near real time should also be considered a unique feature of this technology. The combination of near real-time adjustable, highly dynamic energy distribution and its influence on the weld pool behaviour in stainless steel is therefore a major research gap, building upon which, more in-depth investigations can be carried out considering individual aspects of the CBC laser system. This work is intended to lay the foundation for future work in this area. In contrast to previous work, novel evaluation methods will be used to demonstrate the influence of CBC lasers on capillary geometry—notably in real time—using high-speed imaging and complex measurement techniques. In summary, CBC represents a promising approach for reducing welding defects and enhancing weld seam quality. This study aims to systematically investigate the influence of various beam shapes and modulation frequencies on key process characteristics

of laser beam welding. Particular attention is paid to weld seam geometry, penetration depth, microstructural evolution, and the dynamic behaviour of the vapour capillary—all of which serve as indicators of process stability and energy input distribution.

2. Materials and Methods

The flowchart summarizes the overall methodology and structure of this work (Figure 1). In this study, high-alloy austenitic steel (1.4301) and Duplex steel measuring 100 × 50 × 4 mm were employed as the base materials for welding. Austenitic steel was chosen due to its known susceptibility to solidification cracking (hot cracking) during welding, primarily caused by its low thermal conductivity. Duplex steel, on the other hand, was selected for its thermally sensitive and complex dual-phase microstructure. Varying heat input during welding can alter the ferrite–austenite phase balance, directly affecting its corrosion resistance. These contrasting thermal and metallurgical characteristics make both steels ideal test materials for investigating the influence of beam shape and frequency on weld quality parameters such as hot cracking, grain structure, and weld pool dynamics.

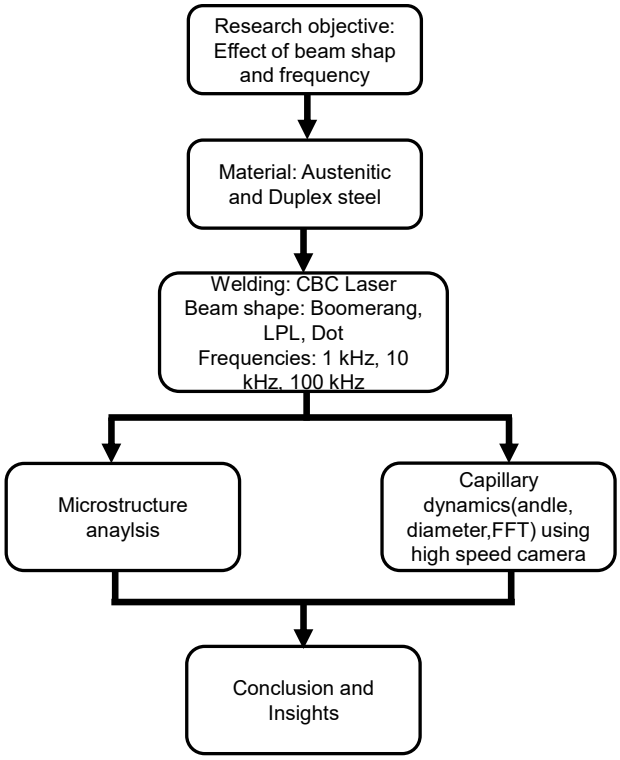


Figure 1. Research workflow overview.

The welding was performed with the help of a CIVAN High Power Single Mode CW Dynamic Beam Laser, which delivers laser radiation with a wavelength of 1064 nm in an optical phased array by combining multiple single mode fibre lasers. In this work, three beam shapes were generated—namely dot, boomerang and line-point-line (LPL). Where the dot is a continuous weld (CW) and the other two beam shapes are oscillated in the frequency range of 1, 10, and 100 kHz, as depicted in Figure 2. A laser power of 6 kW and a welding speed of 2 m/min were used for all the trials (Table 2).

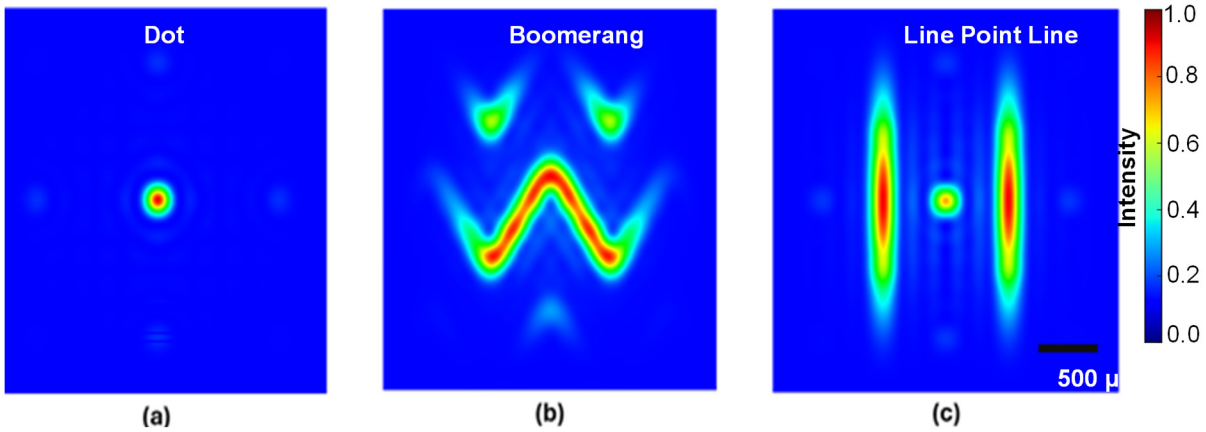


Figure 2. Dynamically generated laser beam with the shapes—(**a**) dot, (**b**) boomerang and (**c**) LPL.

Table 2. Welding parameters with beam shape and frequency.

Material	Beam Shape [-]	Frequency [kHz]	Power [kW]	Welding Speed [m/min]
Austenitic steel/Duplex steel	Dot	CW	6	2
	Boomerang	1, 10, 100	6	2
	LPL	1, 10, 100	6	2

To investigate the influence of beam shape and oscillation frequency on capillary dynamics during laser welding, a high-speed camera (Photron SA4, Photron Limited, Tokyo Japan) was employed to capture the weld process from multiple perspectives. All recordings were conducted at a frame rate of 10,000 to 100,000 frames per second (fps).

To analyse capillary fluctuations and the capillary diameter of the weld seam, bead-on-plate welds were performed at the centre of the specimen, and the camera was positioned at an inclined top-view angle relative to the welding axis (Figure 3a). This setup enabled visualization of the capillary opening and capillary diameter during beam oscillation. To examine the capillary front and its angular orientation, an edge-welding configuration was implemented. In this setup, welding was performed along the edge of the plate, which was optically coupled with a 5 mm thick quartz glass window. This allowed side-view imaging of the capillary front through the transparent medium (Figure 3b), ensuring unobstructed visualization of the capillary inclination and front-wall stability under varying beam conditions. These imaging configurations provided critical insights into the interaction between beam modulation parameters and capillary dynamics, which are directly correlated with weld stability and defect formation.

High-speed imaging data acquired using the Photron SA4 high-speed camera were post-processed using custom MATLAB 2024a scripts to extract quantitative information about capillary dynamics and capillary geometry.

a. Capillary Fluctuations:
To investigate the dynamic behaviour of the capillary, it was hypothesized that the capillary opening and closing would be influenced by the corresponding beam oscillation. Whenever the capillary opens, the laser radiation would enter it and be scattered by the vapour particles present. This scattering would result in a periodic change in the intensity of the pixels within the capillary. A MATLAB script was written to quantify this behaviour, calculating the cumulative intensity of all the pixels grayscale values within the region of interest where the vapour capillary was formed. The cumulative sum of the grayscale values was then plotted against

the frame number, depicting the time axis. Finally, a fast Fourier transform was performed on the intensity change data to identify the dominant frequencies.

b. Capillary front wall inclination:
It is known that the capillary front wall exhibits a change in its angle as the workpiece experiences a translative motion relative to the incident laser. To be able to quantify the same, a MATLAB code was written to reduce the noise in the video playback and binarize the frame data to highlight the vapour capillary. The code then identified the left boundary of the capillary and used the RANSAC algorithm to fit a line to the identified boundary points, as seen in Figure 4. The slope of the line was then plotted per frame. An angular constraint between 60° and 90° from the horizontal was set to avoid fluctuations arising due to noisy data.

c. Capillary dynamics:
The dynamics of the welding process are governed by the fluctuation of the capillary shape. So, avoiding the occurrence of defects in the seam by means of controlling the capillary stability is of significance. A MATLAB script was written to automatically track and analyse the capillary region from the high-speed videos. It processes grayscale frames, segments the capillary based on intensity characteristics as seen in Figure 5, tracks its area and thereby its diameters over time, and performs an FFT analysis on the change of diameter data. The underlying assumption here is that the capillary is circular, to meaningfully manipulate the diameter data to find its dependency on beam shape and oscillation frequency.

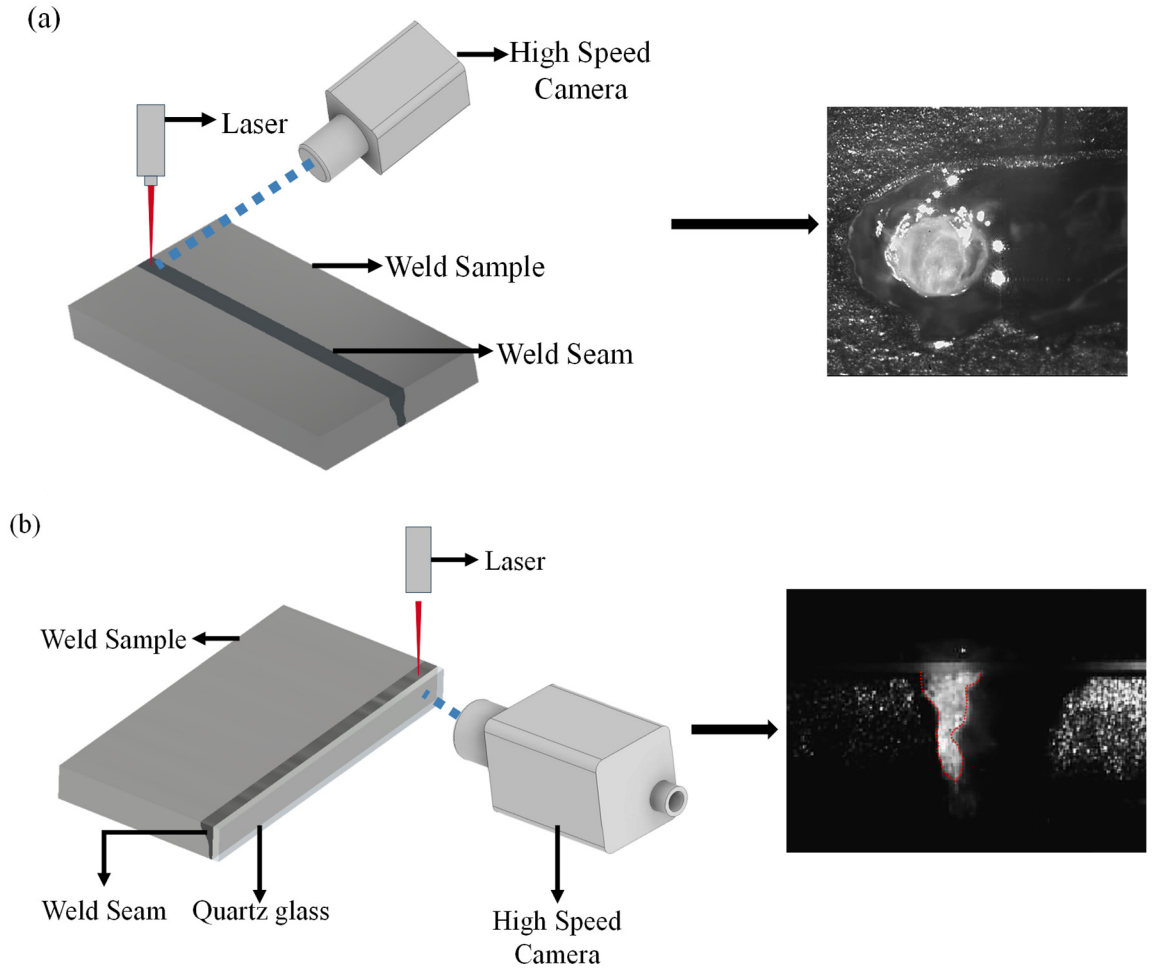


Figure 3. Experimental setup of the laser welding process with high-speed camera—(**a**) Camera positioned at an inclined top-view angle, (**b**) Camera positioned horizontal to the weld.

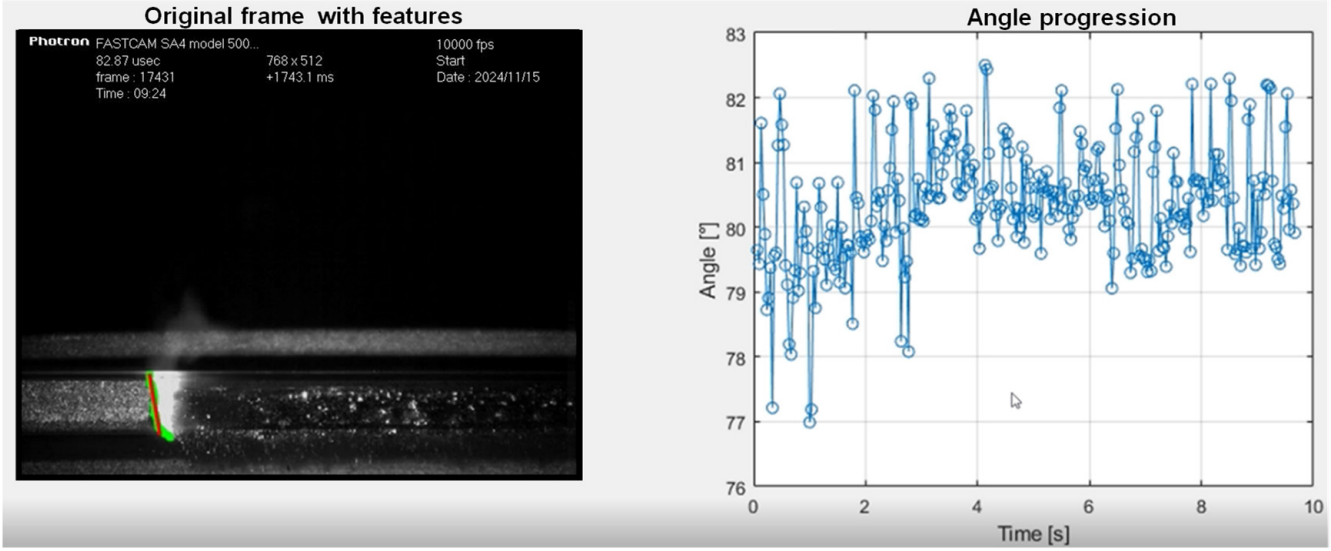


Figure 4. Identified points for the capillary front (green) and fitting line (red) (**left**) and the angle between the fitted line and the horizontal plotted over time (**right**).

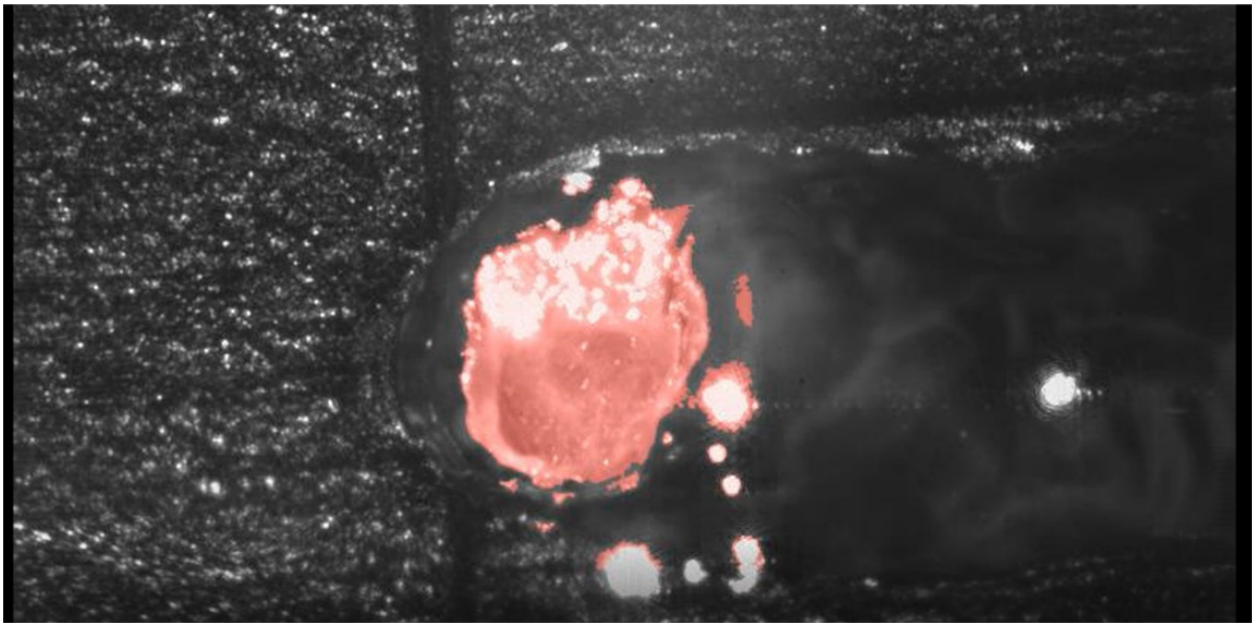


Figure 5. Capillary isolation using MATLAB script.

In addition, metallographic cross-sections were prepared to analyse the weld seam geometry and to establish correlations with the applied dynamic beam parameters. The cross sections are arranged in a matrix format, where the vertical column represents the steel and beam shape, and the horizontal row represents the frequency (Figure 6). As the frequency does not have any major implications for the dot beam shape, the cross section that represents the dot was welded with a 1 kHz beam frequency. The first image of the dot is austenitic steel, and the second is duplex steel.

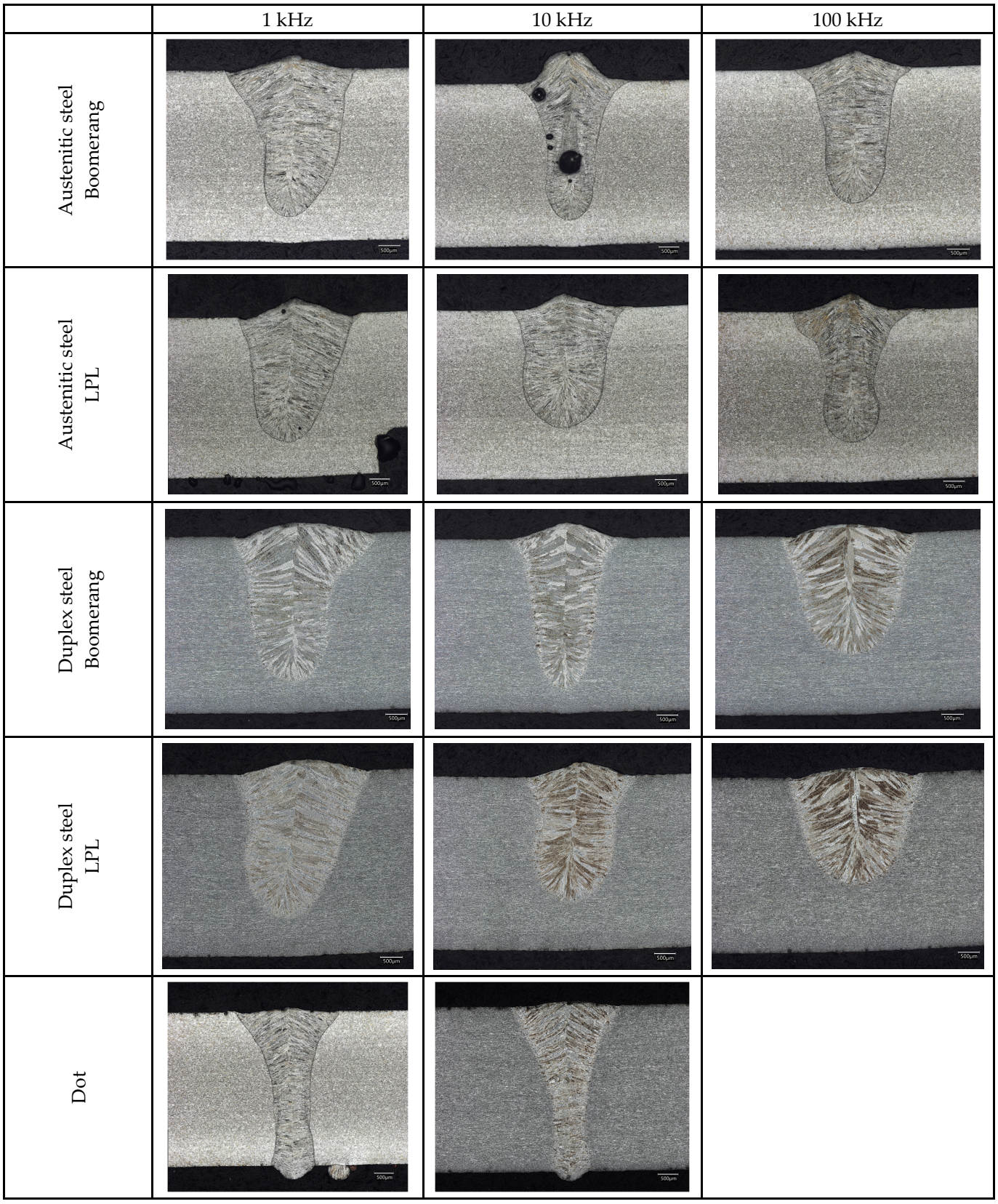


Figure 6. Weld seam cross-section for austenitic and duplex steel using a dynamically generated laser beam.

3. Results and Discussion

This section presents a comprehensive analysis of the effects of beam shape and frequency on weld seam geometry, microstructural evolution and capillary dynamics during laser welding of austenitic and duplex stainless steels using a CBC laser source. The findings are derived from a combination of metallographic cross-section analysis, high-speed imaging, and quantitative post-processing of the acquired data. Key parameters such as capillary fluctuations, capillary diameter, front wall inclination, and weld depth are examined in relation to the applied beam modulation conditions. Preliminary microstructural observations are also correlated with different beam configurations.

3.1. Effect of Beam Shape and Frequency on Weld Seam Geometry

The geometry of the weld seam is significantly influenced by both beam shape and oscillation frequency. To ensure a comparative study, the welding parameters were kept constant across all beam shapes, frequencies, and materials. As illustrated in Figure 6, for both austenitic and duplex steels, the dot beam shape results in a narrow and deep capillary, producing through-penetration welds. This is attributed to the localized energy concentration inherent to the dot shape. In contrast, the boomerang and LPL shapes distribute the energy over a wider area, leading to shallower and less penetrative welds under the same conditions.

As the oscillation frequency increases from 1 kHz to 10 kHz, the weld seam becomes more stable. Interestingly, despite the increased frequency, weld depth is maintained or even slightly increased, suggesting that dynamic beam shaping enhances melt pool control without sacrificing penetration. This behaviour is particularly evident in duplex steel, where more uniform heat distribution contributes to smoother weld profiles. However, in austenitic steel using the boomerang shape at 10 kHz, it is observed that the capillary is unstable, leading to the formation of porosity in the weld seam.

At 100 kHz, a significant broadening of the weld seam is observed, especially in duplex steel. This is likely due to the high thermal conductivity property and the reduced beam interaction time per unit area at high frequency, which causes the laser energy to be distributed more evenly across the oscillation path. Consequently, while weld depth slightly decreases, weld width increases, reflecting a shift from deep-penetration to conduction-mode welding.

Furthermore, for the same beam shapes (Boomerang (BR) and LPL) at 100 kHz, austenitic steel exhibits greater weld depth than duplex steel. This can be attributed to the lower thermal conductivity of austenitic steel, which reduces heat dissipation from the fusion zone, enabling higher peak temperatures and deeper penetration. It is also observed that the weld seams are not symmetric, and this is because the beam shape is rotated by 15° due to the mirror structure in the scanner.

A comprehensive overview of the weld seam depth across different beam shapes, frequencies, and materials is presented in Figure 7.

To further understand the mechanisms underlying the observed changes in weld seam geometry presented in Sections 3.1–3.3 explore the microstructural evolution and capillary dynamics, respectively, as a function of beam shape and modulation frequency. These aspects are intrinsically linked to weld formation, as they influence heat distribution, solidification behaviour, and energy absorption efficiency.

The microstructural analysis in Section 3.2 supports the macroscopic weld profile trends by revealing how thermal gradients and cooling rates, governed by beam dynamics, affect grain structure and phase balance. In parallel, the high-speed imaging results in Section 3.3 provide direct insights into capillary behaviour and stability. Together, these

sections provide an understanding of the overall impact of dynamic beam shaping and frequency modulation on the weld seam.

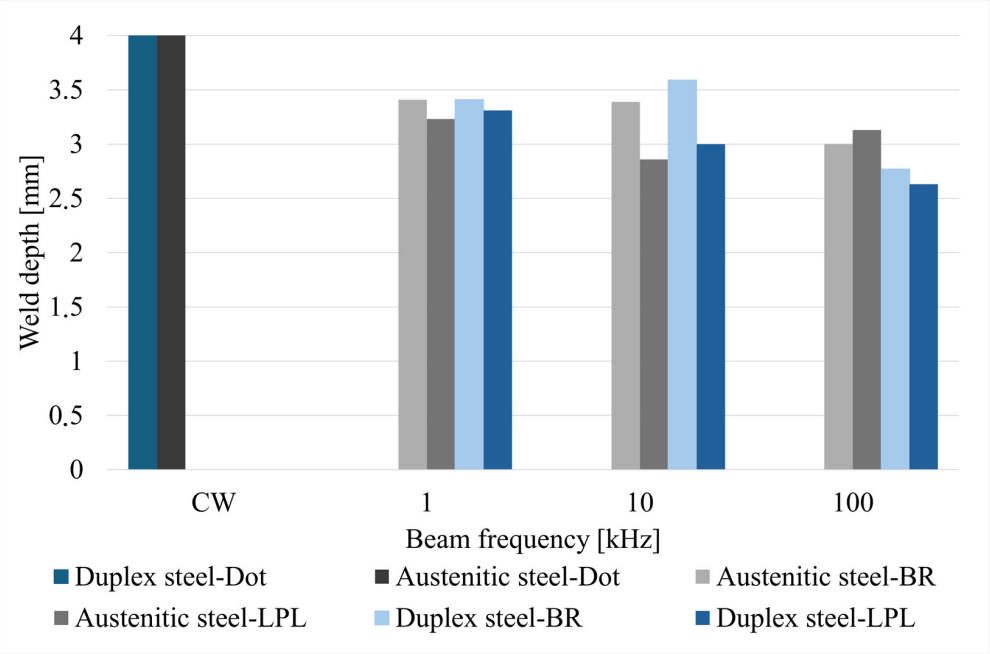


Figure 7. Weld depth comparison for different beam shapes and frequencies.

3.2. Weld Microstructure

Austenitic steel:

The weld zone predominantly consists of columnar austenite with interdendritic delta ferrite. At lower beam frequencies, rapid solidification favoured the formation of fine dendritic grains. As the beam frequency increased, grain size increased significantly due to a decrease in cooling rate. Higher frequencies caused the oscillating beam to broaden the molten pool, extending the solidification time and allowing grains to coarsen. This coarsening effect was most evident in the fusion zone near the weld centre. From Figure 8, the percentage area of the grain boundaries was calculated using ImageJ software (https://imagej.net/ij/, accessed on 18 June 2025). A comparative analysis between the dot and boomerang beam shapes revealed that, with increasing beam frequency, the percentage area of grain boundaries decreased, particularly in the boomerang configuration. This trend is attributed to asymmetric temperature gradients induced by the beam shape. As frequency increased, the molten pool became wider, reducing the local cooling rate at the weld centre. This, in turn, promoted the growth of larger, columnar or coarsened equiaxed grains.

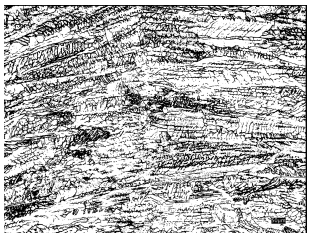
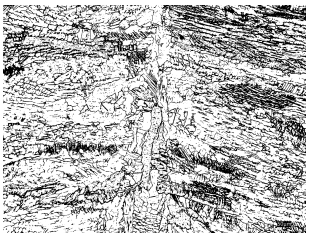
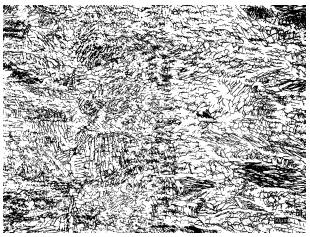
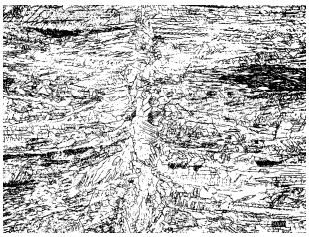
Dot [CW]	Boomerang 1 kHz	Boomerang 10 kHz	Boomerang 100 kHz
			
% of Area: 21.74	% of Area: 14.66	% of Area: 15.80	% of Area: 11.51

Figure 8. Microstructure at the centre of the weld seam for boomerang beam shape.

A similar trend was also noticed in the microstructure generated using the LPL beam shape in the case of 1 and 10 kHz. However, at 100 kHz, a finer equiaxed grain structure is developed as the weld seam geometry changes from a tapered weld seam to a nail head weld seam geometry as seen in Figure 6. This transformation is mainly due to the delivery of a symmetric concentrated energy by the combination of line-point-line, where the point is responsible for the generation of a deeper weld. This deep weld leads to fast cooling, resulting in a finer grain structure as seen in Figure 9. The percentage area of the grain boundary for the LPL beam shape at 100 kHz is found to be the highest (~17.3%) after the dot beam shape (~21.7%).

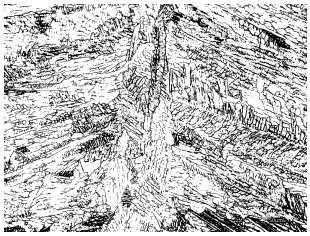
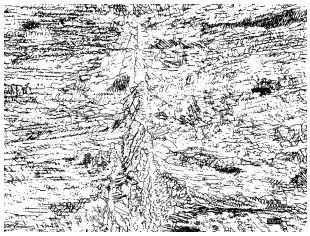
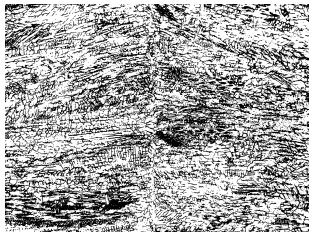
LPL 1 kHz	LPL 10 kHz	LPL 100 kHz
		
% of Area: 8.9	% of Area: 6.36	% of Area: 17.32

Figure 9. Microstructure at the centre of the weld seam for LPL beam shape.

Duplex steel: Duplex steel welds displayed a dual-phase microstructure of ferrite and austenite. At lower beam frequencies, the weld seam showed an acceptable balance between austenite and ferrite in the range of 24.90%–21.21%. However, at high frequencies (100 kHz), reduced cooling rates and altered thermal gradients promoted excessive ferrite at the weld centre. The austenitic phase fraction for both the beam shape and frequencies was calculated using ImageJ software. The highest austenitic phase fraction (28% in the weld seam) was observed using the dot beam shape. The calculated austenitic phase fractions for both beam shapes are illustrated in Figures 10 and 11. Improper phase balance in duplex steel can negatively affect corrosion resistance and mechanical properties. Therefore, it is important to select the beam shape and frequency based on the application.

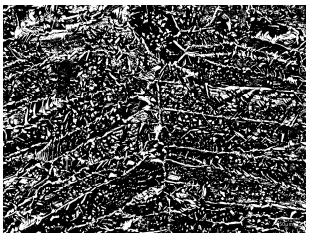
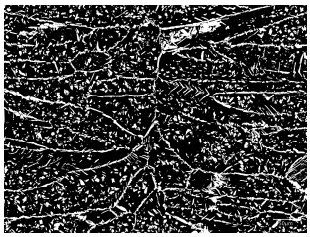
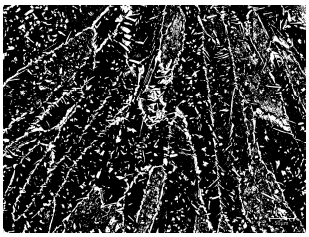
Dot [CW]	Boomerang 1 kHz	Boomerang 10 kHz	Boomerang 100 kHz
			
Austenite fraction: 28%	Austenite fraction: 23.5%	Austenite fraction: 21.5%	Austenite fraction: 20.6%

Figure 10. Microstructure at the centre of the weld seam for boomerang and dot beam shapes.

Overall, the analysis demonstrates that both the beam shape and oscillation frequency significantly influence the local energy density distribution, which in turn affects the seam morphology, microstructure, and penetration profile during welding.

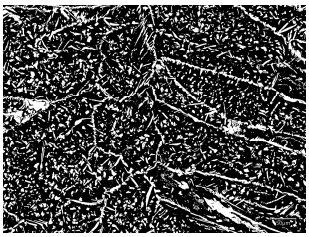
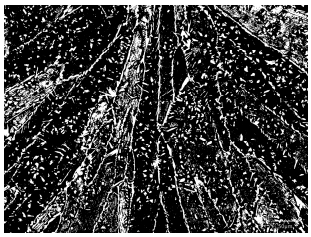
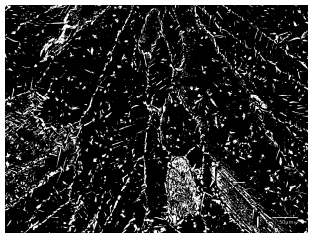
LPL 1 kHz	LPL 10 kHz	LPL 100 kHz
		
Austenite fraction: 24.9%	Austenite fraction: 21.2%	Austenite fraction: 11.9%

Figure 11. Microstructure at the centre of the weld seam for LPL beam shape.

3.3. Influence of Beam Oscillation on Capillary Dynamics and Stability

The dynamic interaction between beam oscillation frequency, beam shape, and capillary behaviour was analysed using high-speed imaging at 10,000 fps and 100,000 fps, enabling time-resolved studies at 1 kHz and 10 kHz modulation frequencies. This allowed for accurate characterisation of the capillary and capillary fluctuations across different material conditions.

Capillary Fluctuations:

For both austenitic and duplex stainless steels, fast Fourier transform (FFT) analysis of the cumulative grayscale intensity within the vapour capillary region revealed distinct frequency peaks at approximately 993 Hz (for 1 kHz oscillation) and 9886 Hz (for 10 kHz oscillation). These frequencies correspond to the periodic opening and closing of the capillary, modulated by the oscillation of the beam. This strongly supports the hypothesis that beam dynamics directly influence energy absorption efficiency by modulating capillary geometry and exposure time, thereby affecting laser–material interaction. Figure 12 shows the FFT of the change in cumulative pixel intensities of the capillary for both 1 kHz and 10 kHz.

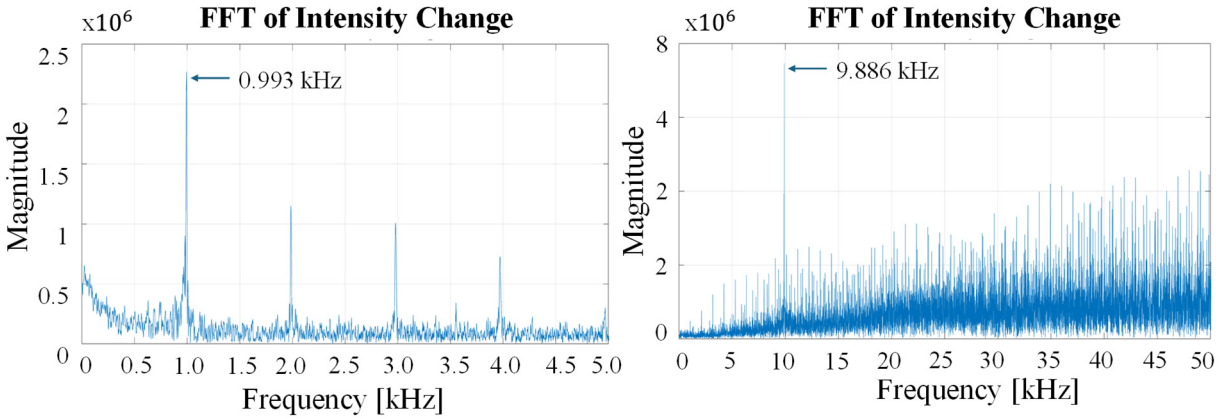


Figure 12. Graph depicting FFT of change in cumulative pixel intensities of the capillary for (**left**) 1 kHz boomerang beam oscillation and (**right**) 10 kHz boomerang beam oscillation.

The FFT-based analysis of grayscale intensity fluctuations is used here as an indirect indicator of capillary dynamics, based on the assumption that increased brightness corresponds to laser radiation entering the vapour capillary during its opening phases, enhanced by internal reflection and scattering within the keyhole. However, this interpretation has inherent limitations. Other dynamic phenomena, such as metal vapour formation, recoil pressure-induced melt pool motion, and thermal radiation, can also contribute to pixel intensity variations. Ideally, isolating these individual effects requires complementary

diagnostics, such as thermal imaging or Schlieren-based techniques, to distinguish between capillary behaviour and plume dynamics. Further work is focused on correlating intensity fluctuations with independent measurements of plume behaviour to refine this interpretation. Despite these limitations, the current approach offers a reasonable first-order approximation of capillary dynamics in response to beam modulation.

In parallel, the inclination angle of the capillary front wall was extracted frame-by-frame using MATLAB-based image analysis. The inclined wall geometry enhances absorption via repeated Fresnel reflections, which increases the effective path length of the laser inside the material. In this study, an increase in beam oscillation frequency for both the boomerang and line-point-line (LPL) beam shapes resulted in a positive capillary front angle, indicating a forward tilt of the capillary wall in the direction of welding. At lower frequencies (1 kHz), the capillary angle approached 0° (neutral), which was particularly evident in the dot beam configuration. This neutral orientation led to deeper penetration, attributed to the maximised recoil pressure acting directly downward into the material. In contrast, at higher frequencies, the positive capillary angle distributed energy over a wider area, promoting shallower penetration, greater capillary fluctuation, and wider melt pools. FFT analysis of the inclination angle also revealed the oscillation frequency as the dominant component, confirming that the beam motion also modulates the capillary front wall. This directly links beam oscillation to capillary shape evolution, further impacting melt pool dynamics and heat input localisation Figure 13.

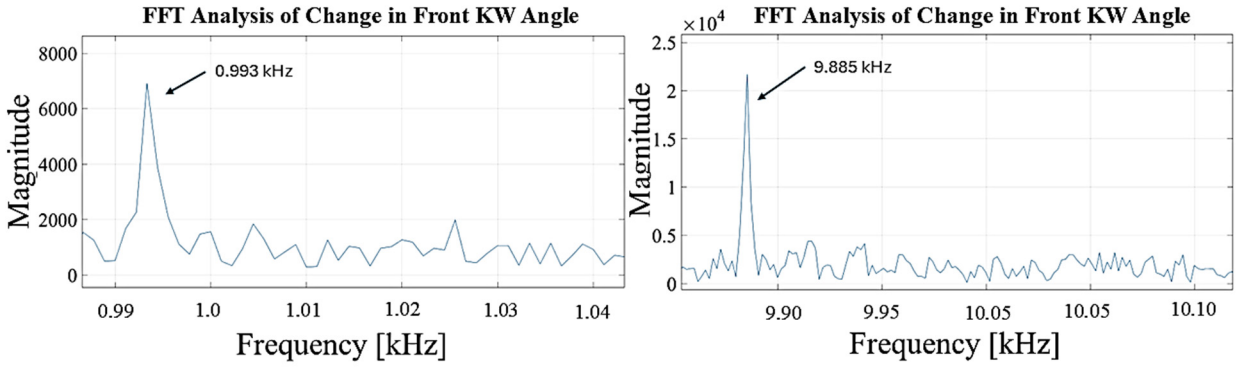


Figure 13. Angle of deflection of the capillary front as a function of frame number (**left**) and Fast Fourier Transform of the change in the angle (**right**).

Capillary diameter and beam shape dependence:

The capillary diameter was plotted as a function of beam shape and oscillation frequency. Among the tested shapes: dot, LPL, and boomerang, the LPL and dot configurations consistently exhibited larger capillary diameters, while the boomerang shape resulted in a smaller and more constricted capillary. This is attributed to the greater area coverage of the LPL shape, distributing energy over a broader region and producing a wider melt pool. Conversely, the dot shape focuses energy at a single point, increasing localised vaporisation and thereby creating a deep and wide capillary Figure 14.

Additionally, a clear inverse relationship was observed between capillary diameter and oscillation frequency. At lower frequencies, the beam dwells longer, allowing higher localised heat input and wider capillary formation. As the frequency increases, the energy input becomes more temporally distributed, leading to narrower and more stable capillaries. FFT analysis of the diameter variations over time further confirmed the presence of the beam oscillation frequency as a dominant spectral component, indicating a direct modulation of capillary stability and size by the laser dynamics Figure 15.

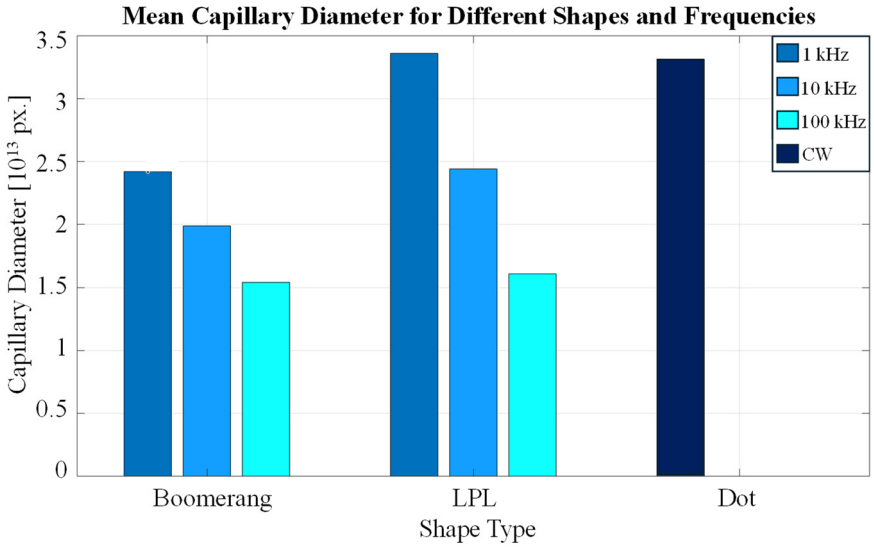


Figure 14. Capillary diameter as a function of beam shape and oscillation frequency.

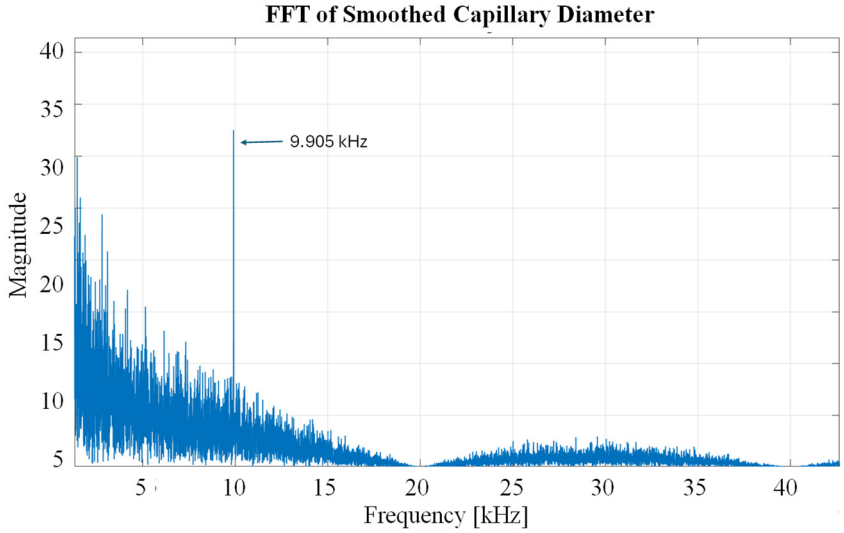


Figure 15. FFT of the capillary diameter for "LPL" beam shape with 10 kHz oscillation frequency.

These findings confirm that beam shape and frequency modulation significantly affect both capillary dynamics and capillary morphology, directly influencing the energy absorption characteristics, melt pool stability and, ultimately, weld quality.

Custom MATLAB-based tools were developed to analyse capillary dynamics from high-speed video data. Although not benchmarked against commercial software, internal validation was performed by manually tracking selected frames and comparing capillary diameter and centroid position. Edge detection and thresholding parameters were optimised based on known visual features, such as capillary contrast and beam reflection. Future work will include systematic benchmarking against independent methods to enhance reproducibility and comparability.

4. Summary and Outlook

This study investigates the effect of beam shape and oscillation frequency on weld quality, capillary dynamics, and microstructure during laser welding of austenitic (1.4301) and duplex stainless steels using a high-power Coherent Beam Combining (CBC) laser system. Advanced diagnostics, including high-speed imaging and metallographic analysis, were employed to understand how dynamic beam modulation influences material behaviour.

- Capillary Dynamics:
  High-speed imaging from top and side views revealed that capillary behaviour—such as opening, closure, and front wall inclination—varies significantly with oscillation frequency. Higher frequencies induced greater capillary fluctuations, especially in austenitic steel. FFT analysis confirmed that capillary oscillation matched the imposed modulation frequencies, indicating a dynamic material response.
- Capillary Diameter and Penetration Depth:
  Image analysis showed a reduction in capillary diameter with increasing frequency, due to more localised and transient energy input. However, penetration depth increased for specific beam shapes and frequencies, highlighting improved energy coupling under certain dynamic conditions.
- Microstructure and Weld Geometry:
  Metallographic cross-sections revealed beam shape and frequency-dependent changes in weld morphology and phase composition. In austenitic steel, higher frequencies promoted grain coarsening, while in duplex steel, increased frequency shifted the ferrite–austenite balance toward ferrite. Weld geometry transitioned from narrow–deep to wide–shallow in duplex steel with LPL beam shapes, whereas the opposite trend was observed in austenitic steel.

These results demonstrate that beam shape and frequency modulation can significantly influence energy delivery, melt pool behaviour, and final weld properties. Future work will explore correlations with residual stress, mechanical performance, and microstructural evolution using EBSD, TEM, and SPH-based numerical modelling to deepen the understanding of the process–structure–property relationships in dynamically modulated laser welding.

Author Contributions: K.R.K.M.: Writing—review & editing, Writing original draft preparation, Conceptualization, Methodology, Visualization, Investigation, Validation. R.S.: Writing introduction, Investigation. A.S.: Data curation, MATLAB scripts. S.O.: Project administration, U.R.: Project administration, funding acquisition. All authors have read and agreed to the published version of the manuscript.

Funding: This research was funded by the Deutsche Forschungsgemeinschaft e.V. (DFG, German Research Foundation). The sponsorship and support are gratefully acknowledged.

Institutional Review Board Statement: Not applicable.

Informed Consent Statement: Not applicable.

Data Availability Statement: The research data have been uploaded in the link below and will be made available upon request: http://hdl.handle.net/21.11102/1b9659b4-9392-4cbe-9a60-1096e6800816 (accessed on 18 June 2025).

Acknowledgments: The presented investigations were carried out at RWTH Aachen University Welding and Joining Institute ISF within the framework of the Collaborative Research Centre SFB1120-236616214 “Bauteilpräzision durch Beherrschung von Schmelze und Erstarrung in Produktionsprozessen”.

Conflicts of Interest: The Authors have no conflicts of interest to declare.

References

1. *Laser Welding MDPI*; Oliveira, J.P., Ed.; MDPI: Basel, Switzerland, 2020; ISBN 978-3-03928-862-5.
2. Klimpel, A. Review and Analysis of Modern Laser Beam Welding Processes. *Materials* **2024**, *17*, 4657. [CrossRef]
3. Möbus, M.; Pordzik, R.; Seefeld, T. Influence of intensity distributions on the process dynamics during laser deep penetration welding of pure nickel with a flexible ring mode laser source. *J. Laser Appl.* **2024**, *36*, 042073. [CrossRef]

4. Schiry, M.; Plapper, P. Influence of laser parameter on weld bead shape and process stability of laser welded steel sheets. In Proceedings of the 10th Conference on Photonic Technologies LANE 2018, Fürth, Germany, 3–6 September 2018.
5. Suder, W.; Chen, X.; Sierra, D.R.; Chen, G.; Wainwright, J.; Rajamudili, K.; Pardal, G.R.; Williams, S. Control of meltpool shape in laser welding. *Weld. World* **2024**, *68*, 1485–1495. [CrossRef]
6. Gong, S.; Pang, S.; Wang, H.; Zhang, L. (Eds.) *Weld Pool Dynamics in Deep Penetration Laser Welding*; Springer: Singapore, 2021; ISBN 978-981-16-0788-2.
7. Dittrich, D.; Keßler, B.; Strohbach, R.; Jahn, A. Laser beam welding of hot crack sensitive Al-alloys without filler wire by intensity controlled dynamic beam oscillation. *Procedia CIRP* **2022**, *111*, 435–438. [CrossRef]
8. Dittrich, D.; Börner, S.; Larrañaga, J.B.; Sahm, T.; Jahn, A.; Wetzig, A. Coherent beam combining—Beam characterization of a new 14 kW CBC laser source and first results on copper welding. *Procedia CIRP* **2024**, *124*, 724–729. [CrossRef]
9. Weber, R.; Wagner, J.; Peter, A.; Hagenlocher, C.; Spira, A.; Urbach, B.; Shekel, E.; Vidne, Y. Basic Properties of High-Dynamic Beam Shaping with Coherent Combining of High-Power Laser Beams for Materials Processing. *JMMP* **2025**, *9*, 85. [CrossRef]
10. Shekel, E.; Vidne, Y.; Urbach, B. 16kW single mode CW laser with dynamic beam for material processing. Fiber Lasers XVII: Technology and Systems. *SPIE* **2020**, *11260*, 267–272. [CrossRef]
11. Wagner, J.; Leis, A.; Armon, N.; Nissenbaum, A.; Hagenlocher, C.; Holland, J.; Weber, R.; Graf, T. Coherent beam combining—unlimited flexibility in laser material processing. *PhotonicsViews* **2022**, *19*, 60–63. [CrossRef]
12. Sawannia, M.; Wagner, J.; Stritt, P.; Ramsayer, R.; Hagenlocher, C.; Graf, T. Response of the melt pool and vapour capillary on dynamic beam shaping in the kHz regime during laser welding. *Procedia CIRP* **2024**, *124*, 430–433. [CrossRef]
13. Olschok, S.; Troise, M.; Reisgen, U. Laser beam welding of high thickness sheet metal with highly dynamic beam shaping. *Procedia CIRP* **2024**, *124*, 733–736. [CrossRef]
14. Berger, P.; Hügel, H.; Graf, T. Understanding Pore Formation in Laser Beam Welding. *Phys. Procedia* **2011**, *12*, 241–247. [CrossRef]
15. Brinkmeier, D.; Wagner, J.; Sawannia, M.; Wahl, J.; Menold, T.; Stritt, P.; Ramsayer, R.; Graf, T.; Michalowski, A. Influence of the laser-plume interaction on the beam profile during deep-penetration welding with coherent beam shaping. *Opt. Express* **2025**, *33*, 2702–2711. [CrossRef]
16. Wahl, J.; Frey, C.; Powell, J.; Zaiß, F.; Haas, M.; Olschok, S.; Reisgen, U.; Hagenlocher, C.; Graf, T. Laser-plume interactions in deep-penetration remote laser welding of stainless steel. *Opt. Laser Technol.* **2025**, *186*, 112678. [CrossRef]
17. Zaiß, F.; Haas, M.; Powell, J.; Wahl, J.; Diegel, C.; Schricker, K.; Bergmann, J.P.; Hummel, M.; Spurk, C.; Olowinsky, A.; et al. Reducing capillary depth fluctuations in high-speed laser welding of stainless steel using multi-core laser technology. *Procedia CIRP* **2024**, *124*, 413–417. [CrossRef]
18. Xie, W.; Tu, H.; Nian, K.; Zhang, D.; Zhang, X. Microstructure and mechanical properties of Flexible Ring Mode laser welded 304 stainless steel. *Opt. Laser Technol.* **2024**, *174*, 110563. [CrossRef]
19. Zaißa, F.; Haasa, M.; Wagnera, J.; Diegelb, C.; Schrickerb, K.; Bergmannb, J.P.; Hummel, M.; Olowinski, A.; Beckmann, F.; Moosmann, J.; et al. *Influence of Capillary SHAPE on spatter Formation During Welding with Ring-Core Fiber Systems*; Lasers in Manufcaturing Conference 2023; Helmholtz-Zentrum Hereon: Geesthacht, Germany, 2023.
20. Nahr, F.; Bartels, D.; Rothfelder, R.; Schmidt, M. Influence of Novel Beam Shapes on Laser-Based Processing of High-Strength Aluminium Alloys on the Basis of EN AW-5083 Single Weld Tracks. *JMMP* **2023**, *7*, 93. [CrossRef]
21. Wagner, J.; Heider, A.; Ramsayer, R.; Weber, R.; Faure, F.; Leis, A.; Armon, N.; Susid, R.; Tsiony, O.; Shekel, E.; et al. Influence of dynamic beam shaping on the geometry of the keyhole during laser beam welding. *Procedia CIRP* **2022**, *111*, 448–452. [CrossRef]
22. Kayahara, T.; Tanabe, T.; Sato, Y.; Takenaka, K.; Tsukamoto, M. Effects of beam shape formed by beam-splitting diffractive optical element on keyhole and molten pool behavior in high-power laser welding of stainless steel. *J. Laser Appl.* **2025**, *37*, 032014. [CrossRef]
23. Börner, S.; Dittrich, D.; Barrios Laranaga, J. Enhanced Process Understanding for Laser Welding of Copper and Aluminum Alloys with Dynamic Beam Oscillation. In Proceedings of the Lasers in Manufacturing Conference, Munich, Germany, 26–29 June 2023.
24. Ai, Y.; Yan, Y.; Han, S. Numerical Analysis of Molten Pool Dynamic Behaviors during High-Speed Oscillation Laser Welding with Aluminum Alloy. *Metals* **2024**, *14*, 192. [CrossRef]
25. Berger, P.; Heider, A.; Boley, M.; Förster, D. (Eds.) *Capillary Geometries During Welding of Metals Observed with X-Ray Technique and Calculated Using a Ray-Tracing Tool and a Finite Volume Program Treating Heat Diffusion and Fluid Flow*; Proceedings of the LiM; Institut für Strahlwerkzeuge: Stuttgart, Germany, 2015.
26. Börner, S.; Dittrich, D.; Sahm, T.; Ullmann, L.; Kamm, P.H.; Jahn, A. X-ray analysis of capillary and melt pool dynamics using laser beam oscillation welding for aluminum die-casts. *J. Laser Appl.* **2025**, *37*, 022019. [CrossRef]
27. Kang, S.; Joonghan, S. The effect of laser beam intensity distribution on weld characteristics in laser welded aluminum alloy (AA5052). *Opt. Laser Technol.* **2021**, *142*, 107239. [CrossRef]
28. Song, D.; Kim, R.; Choi, K.; Shin, D.; Lee, S. Effects of Beam Shape on the Microstructures and Mechanical Properties during Thin-Foil Laser Welding. *Metals* **2023**, *13*, 916. [CrossRef]

29. Zeng, X.; Lu, C.; Zhu, Q.; Cui, X.; Li, Z.; Shi, W.; Zhang, R.; Liu, X.; Di, T. Effect of Oscillating Amplitude on Microstructure and Mechanical Property of Laser Welding of Dissimilar Stainless Steel. *Coatings* **2024**, *14*, 1617. [CrossRef]
30. Pekkarinen, J.; Veli, K. The effects of laser welding parameters on the microstructure of ferritic and duplex stainless steels welds. *Phys. Procedia* **2010**, *5*, 517–523. [CrossRef]
31. Šimeková, B.; Dománková, M.; Kovaříková, I.; Kovačócy, P.; Martinkovič, M.; Šimek, M.; Ciuła, L. Microstructural and Mechanical Characterization of the Laser Beam Welded SAF 2507 Super-Duplex Stainless Steel. *Metals* **2024**, *14*, 1184. [CrossRef]
32. Lippold, J.C. (Ed.) *Welding Metallurgy and Weldability*; John Wiley & Sons: Hoboken, NJ, USA, 2014; ISBN 9780471473794.

Disclaimer/Publisher's Note: The statements, opinions and data contained in all publications are solely those of the individual author(s) and contributor(s) and not of MDPI and/or the editor(s). MDPI and/or the editor(s) disclaim responsibility for any injury to people or property resulting from any ideas, methods, instructions or products referred to in the content.